Materials Research. 2013; 16(3): 597-602
DOI: 10.1590/S1516-14392013005000030

Electrical, Photoelectrical and Morphological Properties of ZnO Nanofiber Networks Grown on SiO_2 and on Si Nanowires

***Nadia Celeste Vega*[a,b], *Monica Tirado*[c]*, *David Comedi*[a,b,c], *Andres Rodriguez*[d], *Tomas Rodriguez*[d], *Gareth M. Hughes*[e], *Chris R. M. Grovenor*[e], *Fernando Audebert*[b,e,f]**

[a]*Laboratorio de Física del Sólido, Departamento de Física, Facultad de Ciencias Exactas y Tecnología – FACET, Universidad Nacional de Tucumán – UNT, Av. Independencia, 1800, (4000) Tucumán, Argentina*
[b]*Consejo Nacional de Investigaciones Científicas y Técnicas – CONICET., Argentina*
[c]*Laboratorio de Nanomateriales y de Propiedades Dieléctricas, Departamento de Física, Facultad de Ciencias Exactas y Tecnología – FACET, Universidad Nacional de Tucumán – UNT, Av. Independencia, 1800, (4000) Tucumán, Argentina*
[d]*Tecnología Electrónica, Escuela Técnica Superior de Ingenieros de Telecomunicación – ETSIT, Universidad Politécnica de Madrid – UPM, 28040 Madrid, España*
[e]*Department of Materials, University of Oxford, Parks Road OXI 3PH, Oxford, UK*
[f]*Grupo de Materiales Avanzados, Facultad de Ingeniería, Universidad de Buenos Aires, Paseo Colón 850, Buenos Aires (1063), Argentina*

Received: November 12, 2012; Revised: December 5, 2012

ZnO nanofibre networks (NFNs) were grown by vapour transport method on Si-based substrates. One type of substrate was SiO_2 thermally grown on Si and another consisted of a Si wafer onto which Si nanowires (NWs) had been grown having Au nanoparticles catalysts. The ZnO-NFN morphology was observed by scanning electron microscopy on samples grown at 600 °C and 720 °C substrate temperature, while an focused ion beam was used to study the ZnO NFN/Si NWs/Si and ZnO NFN/SiO_2 interfaces. Photoluminescence, electrical conductance and photoconductance of ZnO-NFN was studied for the sample grown on SiO_2. The photoluminescence spectra show strong peaks due to exciton recombination and lattice defects. The ZnO-NFN presents quasi-persistent photoconductivity effects and ohmic I-V characteristics which become nonlinear and hysteretic as the applied voltage is increased. The electrical conductance as a function of temperature can be described by a modified three dimensional variable hopping model with nanometer-ranged typical hopping distances.

Keywords: *nanostructures, semiconductors, ZnO, photoluminescence, photoconductivity*

1. Introduction

ZnO nanofiber networks (NFNs) have been of interest in recent years due to their potential in future technological applications[1-7]. ZnO is a n-type semiconductor with a direct wide band gap of 3.37 eV (UV), large exciton binding energy (60 meV), high superficial reactivity and high Curie temperature (with magnetic doping). Therefore, it is a predominant candidate for the development of photonic devices in the UV, like laser, LEDs and photodetectors. When combining the ZnO properties with those inherent of nano-structures, like mechanical flexibility, promising materials for the development of solar cells, sensors, optic memories and basic elements for the construction of flexible and transparent electronics are obtained[4,5,8]. Last but not least, ZnO has high pizoelectricity, which makes it useful for the manufacturing of transductors and small electro-mechanical devices.

The use of low dimensional structures is a key technological factor in the creation of new functional and sensing devices which benefit from their large surface area to volume ratio[7-9]. In addition, there has been interest in achieving Si NW/ZnO NW hybrid devices with enhanced functionality[10] in electronic and photoelectronic properties. Carrier management in hetero-structures could provide ways of enlarging emission wavelength ranges and efficiencies of luminescent devices and also of mastering surface activities in sensors[10].

In this work, we present our study of ZnO NFN samples fabricated on either SiO_2 or Si wafers covered with Si NWs synthesized by low pressure chemical vapor deposition (LPCVD) technique. The morphology and properties of ZnO NFN are strongly dependent on the fabrication conditions, like the substrate temperature. In this work we show how the morphology of the network is modified by changing the substrate temperature from 720 °C to 600 °C, keeping all other growth conditions unmodified. Scanning Electron Microscopy (SEM) images show the morphology of the nanostructure obtained. The interfaces of ZnO NFN/Si NWs/Si and ZnO NFN/SiO_2 were studied with the use of a Dual Beam (FIB/SEM) Microscope.

*e-mail: mtirado@herrera.unt.edu.ar

Photoluminescence, electrical conductance and photoconductance in relation to temperature and to applied polarization voltage were also studied in a sample with ZnO NFN grown on SiO_2 substrate without Si NWs. The conductivity of the ZnO NFN can be represented by two parallel conductors, each of them dominated by Mott mechanism in three dimensions with different parameters.

2. Material and Methods

The substrates used for ZnO NFN growth were two types: (A) 0.5 µm thick thermal SiO_2 on Si (100) and (B) Si (100) covered with Si NWs that had been grown by LPCVD. In all cases, NF growth was promoted by Au nano-clusters deposited on the substrates[11]. These metallic nanoislands act as catalysts for one-dimensional growth (nanowires, nanocolumns) for different systems[4,11-13].

Three ZnO NFN samples (S_0, S_1, S_2) were fabricated by the vapour-transport method. Their growth details are summarized in Table 1. The ZnO NFN sample (S_0) was grown on a SiO_2 substrate at 720 °C. Samples (S_1, S_2) were grown at 720 °C and 600 °C, respectively on Si (100) substrates that had Si NWs on it. The Si NWs had been synthesized by the LPCVD technique at 400 °C for 30 minutes using Si_2H_6 as precursor gas, with a flow ranging from 8 to 2 sccm. The H_2 flow was changed to achieve a total flow rate of 100 sccm and the total pressure was kept constant at 400 mTorr[14].

The vapour-transport deposition of the ZnO NFN was performed in a pumped quartz tube furnace under Ar high purity (99.999%) flow. An alumina crucible containing ZnO and graphite powders (1:1 weight ratio) was placed inside the quartz tube at a position corresponding to the furnace center (1100 °C), while substrates were placed downstream the tube. The quartz tube, 1m long and 3.4 cm external diameter, was placed within the 0.6 m long tubular furnace. The furnace was controlled by a Honeywell DC1010 temperature controller, which allows setting different profiles of variation of temperature. The substrates were placed parallel to the tube axis at 15.7 cm and 17.9 cm distances from the furnace centre, which correspond to different temperatures: 720 °C and 600 °C respectively, due to the natural temperature gradient profile along the tube[13,15].

The quartz tube was purged with Ar until a base pressure of 250 mTorr was obtained (fixed by a small opening of the air inlet valve at maximum pumping speed) and a steady Ar flow was established by controlling the pumping speed through the vacuum valve, raising the pressure in the tube to about 1200 mTorr. The temperature in the centre of the furnace was set at 1100 °C at a heating rate of 25 °C/min. This temperature value was kept constant during 20 minutes and then, the furnace was naturally cooled to room temperature.

Table 1. Samples code and conditions of ZnO deposition.

Sample	S_0	S_1	S_2
Substrate	Au/SiO_2/Si	Si NWs/Si	Si NWs/Si
ZnO Deposition Temperature	720 °C	720 °C	600 °C

Morphology of all samples was characterized by means of SEM obtained in a JSM 6480 LV microscope and in a Zeiss NVision40 Dual Beam (FIB/SEM) microscope. The later technique was also used for studying the ZnO NFN/Si NW/Si and ZnO NFN/SiO_2 interfaces.

The electrical conductance was determined for sample S_0 by applying a DC bias between two Ag contacts formed on the network (separation: 1mm) and measuring the current with 100 µm diameter Cu wires. I-V curves were obtained with two cycles 0 V → 10 V → –10 V → 0 V at room temperature. The sample was attached to a He closed circuit cryostat sample holder, using high vacuum grease. The pressure in the cryostat during the measurements was lower than 1mTorr, obtained with a diffusion pump. The sample resistance at room temperature was 80 KΩ, approximately. A voltage source was used to apply a bias on the sample, while the current was measured by recording with a nano-voltimeter the voltage drop across a test resistor connected in series with the sample.

Photoconductance was also evaluated for sample S_0 by illuminating the area between contacts with ultraviolet radiation (3.1 eV) obtained from a pair of commercial light emitting diodes and observing the changes in the electrical current with respect to the conductance without illumination.

The network conductance was also measured as a function of the sample temperature by applying on the sample a constant voltage in the ohmic (linear) range. It was found that, by applying identical contacts on a SiO_2 substrate with no deposit on it, the substrate conductance is below the detection limit of the measurement equipment used (~10^{-9} Ω^{-1}) and therefore negligible.

Photoluminescence (PL), also in sample S_0, was measured using the 325 nm wave length of a HeCd laser as excitation source, and a CCD (charge-coupled device) spectrometer from Ocean Optics. The measurements of the PL were performed in the 4 K to 300 K temperature range.

3. Results and Discussion

3.1. *Morphology*

SEM images corresponding to sample S_0 are shown in Figure 1. The ZnO nanofibers are curled with ramifications and they conform a sponge-like three-dimensional random network of randomly oriented nanofibers (Figure 1a, b). Figure 1c shows a detail of the ZnO NFN/SiO_2 interface.

Figure 2a clearly shows that in sample S_1 ZnO NFN growth occurs in the regions among Si NWs and not from the Si NWs themselves. The cross section view (Figure 2b) shows Si NWs (of ~140 nm length) embedded in the ZnO network. In Figure 2.c Au islands and a thin Si film are observed. Au islands are localized at the Si film/Si substrate interface. The Si layer is 100 nm thick and corresponds to Si deposition during the LPCVD process.

Figure 3 shows images of sample S_2, which correspond to the lower ZnO growth temperature (600 °C). The ZnO NFN exhibits a higher density than the network obtained at 720 °C (sample S_1, Figure 2). Hence, for 600 °C, the ZnO NFN obtained is a very dense layer of several microns thick, which covers the whole substrate surface. The cross section view (Figure 3c) shows the Au islands and the Si layer as was observed for the sample S_1.

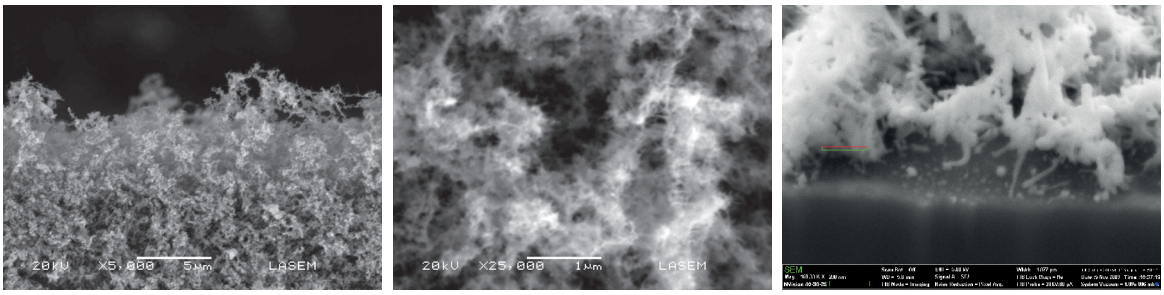

(a) (b) (c)

Figure 1. SEM images of the ZnO NFN of the sample S_0. Image (a) was taken at the edge of the substrate to allow the visualization of the nano-fibres structure. Image (b) corresponds to a cross section view. The interconnected fibres look as a highly porous sponge. In (c) the ZnO NFN deposited on the SiO_2 surface of the substrate is observed.

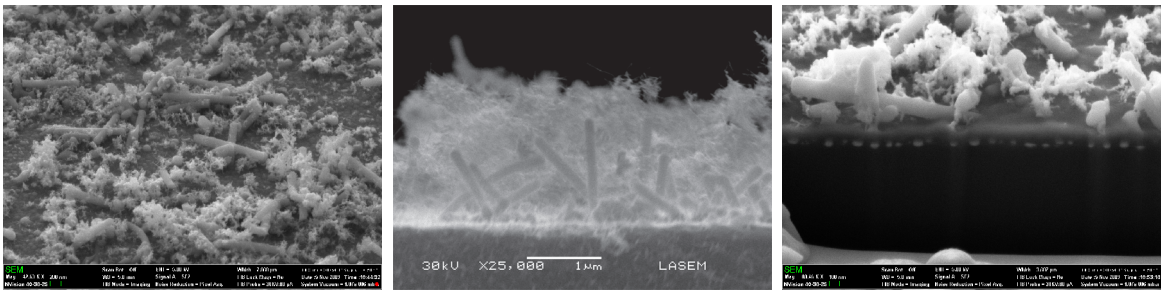

(a) (b) (c)

Figure 2. SEM Images of the ZnO NFN/Si NW of the sample S_1. (a) and (b) correspond to top and edge views. It can be observed that a ZnO NFN grows between the Si NWs and not from them. The ZnO NFN is a highly porous layer filling empty spaces. The diameters range of ZnO NFN is between 10 nm and 20 nm, this is much smaller than the Si NWs diameters (140 nm). Image (b) is cross section view of Si NWs embedded in the ZnO NFN. Image (c) shows a detail of the cross section, where Au islands are observed at the bottom part of the sample. Also a 100 nm thick two-dimensional Si layer deposited on Au nano-clusters can be observed.

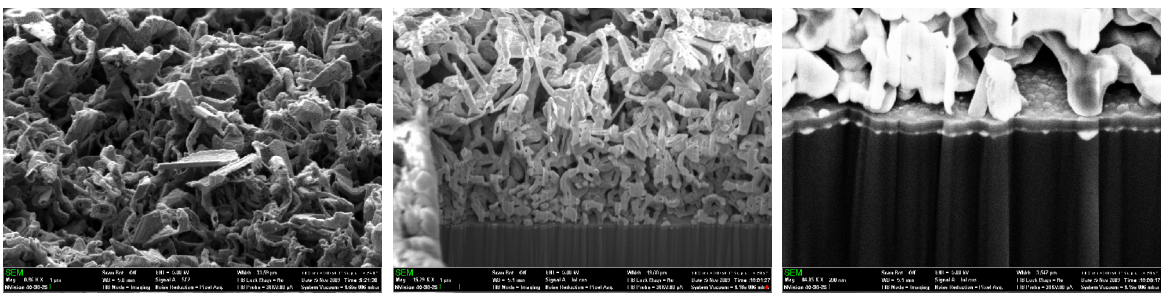

(a) (b) (c)

Figure 3. SEM Images of the ZnO NFN/Si NW of the sample S_2. (a) and (b) correspond to top and edge views. It can be observed that a thick ZnO NFN layer grows fully covering the Si NWs, which therefore cannot be seen in the image. The diameters range of ZnO fibres is between 100 nm and 200 nm. Image (c) shows a detail of the cross section, where Au islands and a 100 nm thick two-dimensional Si layer deposited on Au nanoclusters is observed.

In the three samples studied, the ZnO NFs do not grow in an ordered way, presumably due to a large O vacancy density, as expected in the present oxygen starving deposition conditions. The lack of O_2 could inhibit coherent one-dimensional crystal growth. Studies of ZnO NW growth on SiO_2 with increasing O_2 reveal the development of a 2D ZnO layer (not observed here) followed by an ordered growth of high crystallinity NW vertically aligned[16].

The morphology of the ZnO structure does not seem to strongly depend on the substrate type or the the presence of Au catalyst on the growth surface. This can be seen by comparing Figures 1 and 2, which essentially show very similar ZnO morphologies for samples grown on SiO_2 with Au catalysts as for samples with ZnO grown on Si NW. Note than in the latter case the Au catalysts on the Si (100) were covered by a thin Si film, while some remained at the tip of Si-NWs, as expected from the vapour-liquid-solid mechanism. Nevertheless, the ZnO NFN grew from the regions where Au nanoclusters had been covered and not from the Si NW tips. Furthermore, the presence of Si NWs (and a Si thin film on the areas between the wires as well) did not significantly affect the growth mode. This can be understood by considering that ZnO tends to

grow in a one-dimensional anisotropic way without a metal catalyst due to its polar hexagonal crystalline structure, which favours the ZnO growth along the c axis. In addition, self catalytic growth has also been reported, where Zn clusters act as the catalysts. Indeed, it is very probable that the O_2 starving conditions prevailing in the present experiments favoured the formation of non-oxidized Zn clusters on the SiO_2 and Si substrates.

Further research is clearly needed to understand the growth processes. Future work could concentrate, for instance, on studying the effects of adding an O_2 flux on the resulting ZnO NFN/Si NW morphology. The effect of adding O_2 on the ZnO NWN/SiO_2 has been reported by some of us[15,16].

3.2. *Electrical, photoelectrical and optical characterization*

I-V curves, obtained on sample S_0 at room temperature, change with the cycling of voltage sweeps, producing some hysteresis effects (Figure 4a). Such behavior is typical of oxide semiconductor materials, and has been studied for the development of electronic memories[17].

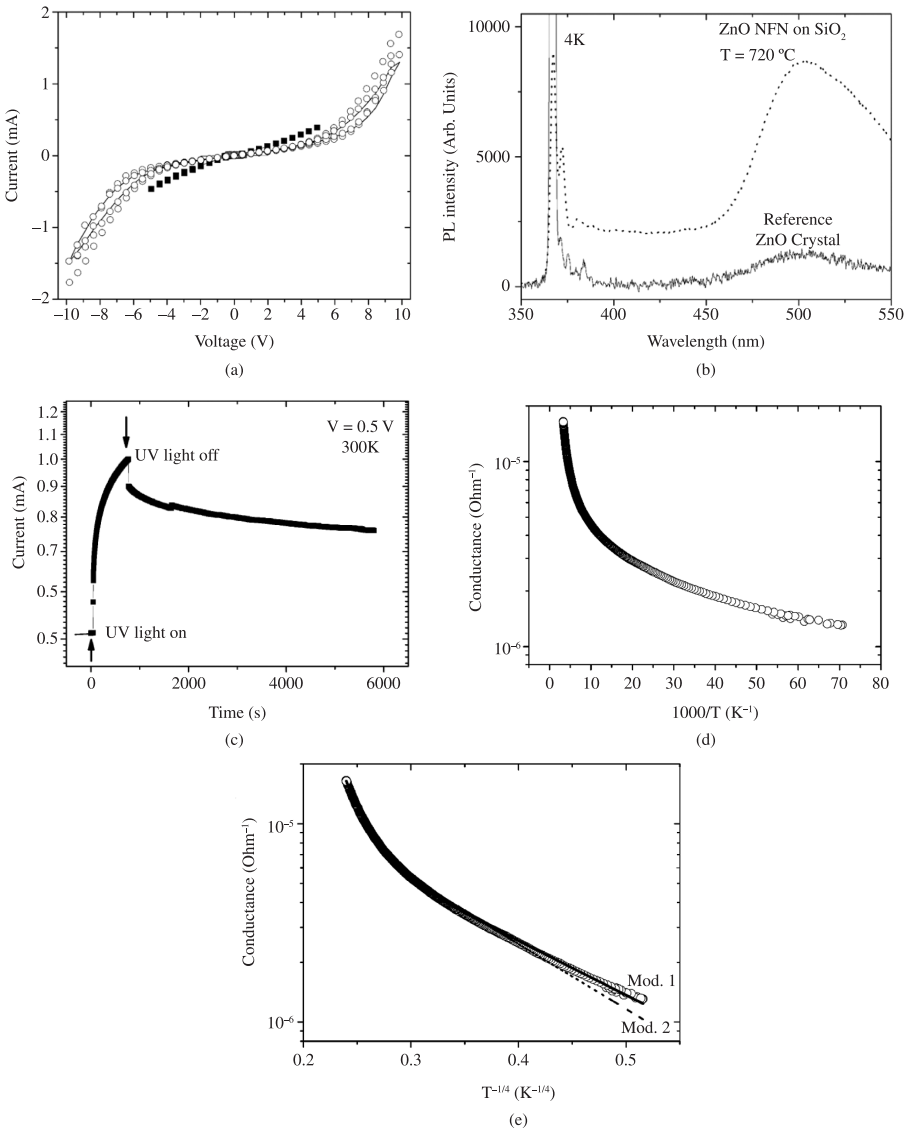

Figure 4. a) I-V curves obtained in sample S_0 with two cycles 0 V → 10 V→ –10 V→ 0 V at room temperature. For $|V| < 4$ V a linear (ohmic) behavior was observed while for values $|V| > 4$ V, nonlinearity and hysteretic behavior occur. (b) Photoluminescence spectrum for the ZnO NFN in sample S_0 at 4 K. Two bands can be observed: a high energy one at 3.4 eV due to excitonic recombinations and a low energy band (~2.5 eV) due to transitions from bandgap defect states. (c) Current through the ZnO network before, during and after UV (3,1 eV) illumination, as a function of time, at 300 K. (d) Conductance (log scale) vs. reciprocal temperature. The conductance increases with temperature, but it does not follow Arrhenius expression ($G \propto Ae^{-Ea/kT}$). The experimental values do not align in a straight line. (e) Conductance (log scale) vs. reciprocal temperature to the power of –1/4. The linear behavior for $T < 70$ K suggests a variable range hopping (VRH) transport mechanism. Model 1 represents the sum of an Arrhenius dependence with a VRH type dependence. Model 2 was calculated by Equation 1.

Photoluminescence spectra from the ZnO NFN typically show a narrow peak in the UV and a broad peak centered in the green wavelength range (see Figure 4b). The UV peak is centered at 367 nm, which corresponds to photon energy of 3.38 eV. This energy corresponds to the ZnO bandgap energy, indicating that this photoluminescence peak results from the recombination of an electron in the conduction band and a hole in the valence band, or from exciton emission. The broad peak is related to recombination of electrons trapped in deep states within the bandgap, due to defects, such as oxygen vacancies or Zn intersticials. The great intensity of this peak indicates that the nanofibers have a large number of defects, which could be related to their large surface area[18].

Photoconductivity effects are observed in the ZnO NFN when the sample is illuminated with UV, as it can be seen in Figure 4c. The energy of the incidental photons (3.1 eV) is a little lower than the ZnO bandgap energy at 300 K (3.3 eV), thus the photons are weakly absorbed in every nanofiber layer, hence penetrating the whole ZnO structure. When interrupting the illumination, photoconductivity has two decay regimes. The first is very fast (characteristic time much lower than a second), and the second one is very slow and non-exponential, which tends to a conductance value a 30% higher than the conductance in initial darkness. This behavior is usually observed in ZnO and other semiconductor oxides films/sheets[18-21], and is explained by the band-band recombination (which occurs in very short times, in the order of 10^{-9} seconds) limited by the extremely slow release of charges from a deep state in the bandgap, due to defects (see Figure 4a).

To measure the electrical resistance as a function of temperature, the applied voltage is kept constant at a value within the ohmic regime (0.5 V) and the temperature is varied in a range 10-300 K. The conductance (G) versus the temperature (T) (Figure 4d) shows a semiconductor behaviour in the sense that G increases with T, however, the dependence does not follow an Arrhenius expression as would be expected for the thermal activation of carriers. In contrast, they can be described by a $\exp(-bT^{-1/4})$, as seen in Figure 4e. Such behaviour is expected in accordance with a conduction mechanism corresponding to variable range hopping (VRH) between localized states in three dimensions[22]. For higher temperatures, T > 70 K, a new mechanism is established, which is characterized by a faster growth of G with T. As it can be seen in Figure 4e, when we tried to represent the conductance behaviour in the whole range of temperatures as the sum of a contribution of a Mott type (which dominates at low T) and another of an Arrhenius type (which dominates at high T), a good fit is not obtained (Model 1). On the contrary, a satisfactory fit is only obtained when the sum of two Mott mechanisms (A and B) is assumed, one at high T and another at low T (Model 2):

$$G \propto \sigma = \sigma_{0A} \exp\left[-\left(T_{0A}/T\right)^{1/4}\right] + \sigma_{0B} \exp\left[-\left(T_{0B}/T\right)^{1/4}\right] \qquad (1)$$

From Mott's VRH expressions[18] we estimated the density of localized states at the Fermi energy (g_F) and the mean hopping distance (R) from the fit values of T_{0A} and T_{0B} (See Table 2). The g_F value obtained for mechanism B is reasonable, but for mechanism A, it is too large. However, it must be remembered that this kind of analysis is known to overestimate g_F in many cases[23]. The R values obtained are significantly smaller than the typical NW diameters (50 nm). This is consistent with the 3D character of the transport revealed by the $T^{-1/4}$ dependence.

Table 2. Values of the density of localized states at the Fermi energy (g_F) and the mean value of the hopping distance (R) from the fit of T_{0A} and T_{0B}.

Mechanism	T_0 (K)	$g_F(eV^{-1}cm^{-3})$	R (nm) 300 K
A	$1{,}6 \times 10^3$	1×10^{22}	0.9
B	$6{,}0 \times 10^6$	4×10^{18}	7

The conductance of the dense ZnO nanofiber network is determined by the conductivity of each nanofiber, the connectivity between them and their density. The conductivity of each of them, at the same time, is probably fixed by the density of O vacancies, as this defect behaves as an n dopant in ZnO[21].

4. Conclusion

Under the present fabrication conditions, the transport in Ar of Zn vapours leads to the formation ZnO NFNs on both, SiO_2/Si and Si NWs/Si substrates whose morphology can be described by three-dimensional networks of interconnected, randomly oriented, curled nanofibers. For high substrate temperature (720 °C) the final product is a sponge-like ZnO structure, while for 600 °C a thick and relatively compact network is obtained. The ZnO NFN/Si NWs/Si samples have the Au islands below a Si thin film, whereas no ZnO thin film could be observed at the ZnO NFN/SiO_2 interface.

ZnO NFN has high photoluminescence and considerable conductance and photoconductance. The conductivity of the ZnO NFN can be represented by two parallel conductors, each of them dominated by Mott mechanism in three dimensions with different parameters. It could be possible that the three-dimensional characteristic of the nanofibers conductivity prevails because their diameter is significantly larger than the average hopping lengths. Also, we speculate that a large vacancy density may be responsible for the disordered character of the NFN, their high PL in the visible, and the hopping conduction. These hypotheses should be verified in future research, together with other possible conductivity models in nanofiber networks.

The network shows quasi-persistent photoconductivity and their I-V characteristics exhibits hysteresis at high V. These properties could be useful for memory applications[17].

The high superficial area in the NFN is also remarkable for the development of ultrasensitive sensors, where the variations of photoconductivity, photoluminescence or conductance could be measured when selected molecules are absorbed at nanofiber walls.

Acknowledgements

This work was partially funded by the Argentinean agencies CONICET, CIUNT 26/E419, FONCyT (PICT 2010 No. 400 and PICT-RAICES No. 2351), MINCyT (Ministerio de Ciencia, Tecnología e Innovación Productiva de la Argentina) and the Spanish Agency AECID.

References

1. Datta N, Ramgir N, Kaur M, Kailasa Ganapathi S, Debnath AK, Aswal DK et al. Selective H_2S sensing characteristics of hydrothermally grown ZnO-nanowires network tailored by ultrathin CuO layers. *Sensors and Actuators B*: Chemical. 2012; 166-167:394-401. http://dx.doi.org/10.1016/j.snb.2012.02.079
2. Ko SH, Lee D, Kang HW, Nam KH, Yeo JY, Hong SJ et al. Nanoforest of Hydrothermally Grown Hierarchical ZnO Nanowires for a High Efficiency Dye-Sensitized Solar Cell. *Nano Letters.* 2011; 11(2):666-671. PMid:21207931. http://dx.doi.org/10.1021/nl1037962
3. Na CW, Woo HS, Kim ID and Lee JH. Selective detection of NO_2 and C_2H_5OH using a Co_3O_4-decorated ZnO nanowire network sensor. *Chemical Communications.* 2011; 47(18):5148-5150. PMid:21416083. http://dx.doi.org/10.1039/c0cc05256f
4. Wang N, Cai Y and Zhang RQ. Growth of nanowires. *Materials Science and Engineering*. 2008; R60:1-51.
5. Unalan HE, Yan Z, Hiralal P, Dalal S, Kuo D, Milne WI et al. Zinc Oxide Nanowire Networks for Macroelectronic Devices. In: *Proceedings of the 8th IEEE Conference on Nanotechnology*; 2008; Arlington, Texas USA; 2008. p. 561-564. http://dx.doi.org/10.1109/NANO.2008.166
6. Al-Heniti S, Badran RI, Umar A, Al-Ghamdi A, Kim SH, Al-Marzouki F et al. Temperature Dependant Structural and Electrical Properties of ZnO Nanowire Networks. *Journal of Nanoscience and Nanotechnology*. 2011; 11:1-7.
7. Yang Q, Guo X, Wang W, Zhang Y, Xu S, Lien DH et al. Enhancing Sensitivity of a Single ZnO Micro-/Nanowire Photodetector by Piezo-phototronic Effect. *ACS Nano*. 2010; 4:6285-6291. PMid:20919691. http://dx.doi.org/10.1021/nn1022878
8. Wang ZL. Self-Powered Nanosensors and Nanosystems. *Advanced Materials*. 2012; 24:280-285. PMid:22329002. http://dx.doi.org/10.1002/adma.201102958
9. Lupan O, Emelchenko GA, Ursaki VV, Chai G, Redkin AN, Gruzintsev AN et al. Synthesis and characterization of ZnO nanowires for nanosensor applications. *Materials Research Bulletin*. 2010; 45:1026-1032. http://dx.doi.org/10.1016/j.materresbull.2010.03.027
10. Rami Reddy Devarapalli RR, Deodatta R. Shinde DR, Barka-Bouaifel F et al. Vertical arrays of SiNWs–ZnO nanostructures as high performance electron field emitters. *Journal of Materials Chemistry.* 2012; 22(43):22922-22928. http://dx.doi.org/10.1039/c2jm34224c
11. Plante MC, Garrett J, Ghosh SC, Kruse P, Schriemer H, Hall T et al. The formation of supported monodisperse Au nanoparticles by UV/ozone oxidation process. *Applied Surface Science*. 2006; 253(4):2348-2354. http://dx.doi.org/10.1016/j.apsusc.2006.05.113
12. Wagner RS and Ellis WC. Vapor-Liquid-Solid Mechanism of Single Crystal Growth. *Applied Physics Letters.* 1964; 4:89-90. http://dx.doi.org/10.1063/1.1753975
13. Comedi D, Tirado M, Zapata C, Heluani SP, Villafuerte M, Mohseni P et al. Randomly Oriented ZnO Nanowires Grown on Amorphous SiO_2 by Metal-Catalyzed Thermal Evaporation. *Journal of Alloys and Compounds*. 2010; 495(2):439-442. http://dx.doi.org/10.1016/j.jallcom.2009.10.070
14. Rodríguez A, Sangrador J, Rodríguez T, Ballesteros C, Prieto AC and Jiménez J. SiGe Nanowires Grown by LPCVD: Morphological and Structural Analysis. *Materials Research Society Symposium Proceedings*. 2010; 1258:P05-05.
15. Vega NC, Wallar R, Caram J, Grinblat G, Tirado M, LaPierre RR et al. ZnO nanowire co-growth on SiO_2 and C by carbothermal reduction and vapour advection. *Nanotechnology.* 2012; 23(27):275602. PMid:22706726. http://dx.doi.org/10.1088/0957-4484/23/27/275602
16. Grinblat G, Capeluto MG, Tirado M, Bragas AV and Comedi D. Hierarchical ZnO nanostructures: Growth mechanisms and surface correlated photoluminescence. *Applied Physics Letters*. 2012; 100:233116. http://dx.doi.org/10.1063/1.4724195
17. Villafuerte M, Juárez G, Heluani SP and Comedi D. Hysteretic Current-Voltage Characteristics in RF-Sputtered nc-TiO_2 Thin Films. *Physica B*. 2007; 398(2):321-324. http://dx.doi.org/10.1016/j.physb.2007.04.035
18. Comedi D, Heluani SP, Villafuerte M, Arce RD and Koropecki RR. Power-law photoconductivity time decay in nanocrystalline TiO_2 thin films. *Journal of Physics*: Condensed Matter. 2007; 19:486205. http://dx.doi.org/10.1088/0953-8984/19/48/486205
19. Moazzami K, Murphy TE, Phillips JD, Cheung MC-K and Cartwright AN. Sub-bandgap photoconductivity in ZnO epilayers and extraction of trap density spectra. *Semiconductor Science and Technology*. 2006; 21:717-723. http://dx.doi.org/10.1088/0268-1242/21/6/001
20. Liao ZM, Lu Y, Zhang JM and Yu DP. Temperature dependence of photoconductivity and persistent photoconductivity of single ZnO nanowires. *Applied Physics A*. 2009; 95:363-366. http://dx.doi.org/10.1007/s00339-008-5058-1
21. Tiwari A, Jin C, Narayan J and Park M. Electrical transport in $ZnO_{1-\delta}$ films: Transition from band-gap insulator to Anderson localized insulator. *Journal of Applied Physics.* 2004; 96:3827-3830. http://dx.doi.org/10.1063/1.1783591
22. Mott NF. Localized states in a pseudogap and near extremities of conduction and valence bands. *Philosophical Magazine*. 1969; 19(160):835:852.
23. Marshall JM and Main C. A new procedure for calculating the density and energy distribution of localized hopping sites in disordered semiconductors, using low-temperature electrical conductivity data. *Journal of Physics*: Condensed Matter. 2008; 20:285210. http://dx.doi.org/10.1088/0953-8984/20/28/285210